

**Study of the Stability of a Direct Stator Current Controller  
for a Doubly-Fed Induction Machine using the Complex  
Hurwitz test**

Journal:	<i>IEEE Transactions on Control Systems Technology</i>
Manuscript ID:	Draft
mstype:	Regular Paper
Date Submitted by the Author:	n/a
Complete List of Authors:	Doria-Cerezo, Arnau; Universitat Politècnica de Catalunya, Electrical Engineering and IOC Bodson, Marc; University of Utah, Electrical and Computer Engineering Batlle, Carles; Universitat Politècnica de Catalunya, Applied Mathematics IV and IOC Ortega, Romeo; CNRS-SUPELEC, LSS
Keywords:	doubly-fed induction machine, Hurwitz test

# Study of the Stability of a Direct Stator Current Controller for a Doubly-Fed Induction Machine using the Complex Hurwitz test

A. Dòria-Cerezo, M. Bodson, C. Batlle and R. Ortega

## Abstract

In this paper, a new control scheme is presented for the doubly-fed induction machine with specific applications to renewable energy (wind farms in particular). The proposed control algorithm offers the advantages of proven stability and remarkable simplicity. In contrast with the classical vector control method, where the doubly-fed induction machine is represented in a stator-flux oriented frame, a model with orientation of the stator voltage is adopted. This uncommon approach allows for a decomposition of the active and reactive powers on the stator side and their regulation on the rotor side. A main contribution of the paper is the use of a Hurwitz test for polynomials with complex coefficients has had little prior application in control theory. This results in a proof that a PI control regulating the stator currents ensures global stability for a feedback-linearized doubly-fed induction machine. The specific condition that the PI gains must satisfy is derived as a simple inequality. The PI controller has a particular structure which directly relates the d-component of the rotor voltages to the q-component of the stator currents and vice-versa. The feedback linearization stage only uses the direct measurement of the rotor and stator currents and is thus easily implementable. Furthermore, it is also shown that the PI controller (without the feedback linearization terms) is also stable for a large range of control gains. Finally, the control system is validated in simulations and in experiments.

## I. INTRODUCTION

Doubly-fed induction machines (DFIM) have become very popular, especially in the field of renewable energy as hybrid engines or high performance storage systems [1][2][3][4] and for wind turbines [5][6][7]. The attractiveness of the DFIM stems primarily from its ability to handle large speed variations around the synchronous speed. Another advantage is that the power electronic equipment that controls the machine only has to handle a fraction of the total power (which is directly related to the operating speed [2]), reducing losses and the cost of the power electronic converter.

In this paper, a typical connection of the DFIM is considered, as shown in Figure 1. In this case, the stator is directly connected to the power grid, while the machine is controlled through the rotor voltages. A back-to-back (B2B) converter, consisting of an AC-DC rectifier and a DC-AC inverter stage, is used for generating the rotor voltages.

For generation, the control goals for a DFIM are usually the active and reactive powers delivered to the grid. For drive applications, the DFIM control is composed of an inner current control loop and an external (and considerably slower) mechanical loop (see in [8] a counter example with a unique control loop). This paper only focusses on the electrical loop, and assumes that, for driving applications, an outer mechanical loop (in terms of torque or speed, depending on the system)

A. Dòria-Cerezo is with the Department of Electrical Engineering and the Institute of Industrial and Control Engineering, Universitat Politècnica de Catalunya, Spain, [arnau.doria@upc.edu](mailto:arnau.doria@upc.edu)

M. Bodson is with the Department of Electrical and Computer Engineering, University of Utah, USA, [bodson@eng.utah.edu](mailto:bodson@eng.utah.edu)

C. Batlle is with the Department of Applied Mathematics IV and the Institute of Industrial and Control Engineering, Universitat Politècnica de Catalunya, Spain, [carles.batlle@upc.edu](mailto:carles.batlle@upc.edu)

R. Ortega is with the Laboratoire des Signaux et Systèmes, Supélec, France, [romeo.ortega@lss.supelec.fr](mailto:romeo.ortega@lss.supelec.fr)

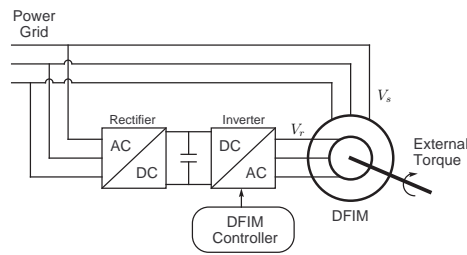


Fig. 1. Typical connection scheme of a DFIM.

provides the active power reference for the electrical controller. The speed is also assumed to vary slower than the electrical variables.

Most DFIM controllers proposed in the literature are based on vector control and decoupling [9][6][10][11], also known as PQ control. The methodology is derived from the description of the electrical part of the DFIM in a stator flux-oriented reference frame which allows the decoupling of the active and reactive powers of the stator side and their independent control through the rotor currents. To achieve the stator flux orientation, the flux angle must be estimated and several complicated operations implemented. In contrast to the stator flux-oriented frame, a model with orientation along the stator voltage vector can be considered [12]. Assuming an infinite bus, control of the stator currents in this reference frame directly translates into the control of the active and reactive powers absorbed or delivered by the machine. Control algorithms are then based on an inner rotor current loop, and an external PQ loop control. Recent examples of this architecture can be found in [13][14].

The main contribution of this paper is the proof that a linear PI control of the stator currents ensures stability for a large range of PI gain values. In comparison with the PQ stator voltage oriented control approaches, the power regulation is achieved with one PI loop, instead of the composition of an outer power regulator and an inner rotor current loop control. Furthermore, global stability can be guaranteed if a feedback linearizing term is added. This feedthrough term only uses the direct measurement of the stator and rotor currents (both accessible for a DFIM), instead of the flux estimation required in the stator flux oriented methods.

The stability proofs are based on a little-known Hurwitz test for complex polynomials [15]. This method allows to significantly reduce the complexity of obtaining the stability conditions by reducing the 6th order characteristic polynomial with real coefficients to a cubic polynomial with complex coefficients. Interestingly, while a Routh-Hurwitz test for the 6th order polynomial of [16] was found to be intractable, application of its version with complex polynomials yields a simple stability test, requiring that a single quadratic inequality be satisfied by the PI gains.

The method proposed in this paper is also applicable to other control problems with certain symmetry properties. In [17], the Hurwitz test was used to find analytic conditions for spontaneous self-excitation in induction generators. The same test was applied to the algorithm presented in [18], see [19].

## II. BACKGROUND: THE COMPLEX HURWITZ TEST

The extension of the well-known Routh-Hurwitz criterion to polynomials with complex coefficients is an old result of the literature [15], possibly not well-known due to the lack of relevant applications. The main result presented in that paper is

summarized by the following Theorem.

*Theorem 1:* The polynomial

$$P(s) = s^n + \alpha_1 s^{n-1} + \alpha_2 s^{n-2} + \dots + \alpha_n \quad (1)$$

where  $\alpha_k = a_k + jb_k$  and  $k = 1, 2, \dots, n$ , has all its zeros in the half-plane  $\Re(s) < 0$  if and only if the determinants,  $\Delta_1 \dots \Delta_k$ ,

$$\begin{aligned} \Delta_1 &= a_1 \\ \Delta_k &= \begin{vmatrix} a_1 & a_3 & a_5 & \dots & a_{2k-1} & -b_2 & -b_4 & \dots & -b_{2k-2} \\ 1 & a_2 & a_4 & \dots & a_{2k-2} & -b_1 & -b_3 & \dots & -b_{2k-3} \\ \vdots & & & \ddots & \vdots & & & \ddots & \vdots \\ 0 & & & \dots & a_k & 0 & & \dots & -b_{k-1} \\ 0 & b_2 & b_4 & \dots & b_{2k-2} & a_1 & a_3 & \dots & a_{2k-3} \\ 0 & b_1 & b_3 & \dots & b_{2k-3} & 1 & a_2 & \dots & a_{2k-4} \\ \vdots & & & \ddots & \vdots & & & \ddots & \vdots \\ 0 & & & \dots & b_k & 0 & & \dots & a_{k-1} \end{vmatrix} \end{aligned}$$

for  $k = 2, 3, \dots, n$  and  $a_r = b_r = 0$  for  $r > n$ , are all positive.

*Proof:* See Theorem 3.2 of [15]. ■

Based on the previous Theorem, the particular case of a cubic polynomial with complex coefficients can be derived.

*Lemma 1:* Assuming that  $a_0$  is real and positive, the roots of a third-order polynomial with complex coefficients

$$P(s) = a_0 s^3 + (a_1 + jb_1)s^2 + (a_2 + jb_2)s + a_3 + jb_3 \quad (2)$$

are in the open left-half plane if and only if  $\Delta_1 > 0$ ,  $\Delta_2 > 0$  and  $\Delta_3 > 0$ , where

$$\Delta_1 = a_1, \quad (3)$$

$$\Delta_2 = \begin{vmatrix} a_1 & a_3 & -b_2 \\ a_0 & a_2 & -b_1 \\ 0 & b_2 & a_1 \end{vmatrix}, \quad (4)$$

$$\Delta_3 = \begin{vmatrix} a_1 & a_3 & 0 & -b_2 & 0 \\ a_0 & a_2 & 0 & -b_1 & -b_3 \\ 0 & a_1 & a_3 & 0 & -b_2 \\ 0 & b_2 & 0 & a_1 & a_3 \\ 0 & b_1 & b_3 & a_0 & a_2 \end{vmatrix}. \quad (5)$$

We will show in Sections IV and V how the complex Hurwitz test can be used to prove stability of a DFIM control law in an elegant and simple manner.

### III. MODEL OF THE DOUBLY-FED INDUCTION MACHINE

The model comes from the three phase dynamical equations of a DFIM, assuming that the machine is symmetric (all windings are identical), the stator-rotor mutual inductances are sinusoidal functions of the rotor angle [20][21], and the three phase system is balanced. These assumptions enable the use of transformations, which greatly simplify the control problem. The basic transformation (also known as Blondel–Park transformation) is widely used in the study of electric machines [21]. This mathematical transformation is used to decouple one of the (balanced) phases, to refer all variables to a common reference frame, and to obtain state-space models whose parameters are independent of the relative angle between rotor and stator.

Similarly to [1] or [2], a transformation to a synchronous frame rotating at the constant frequency of the stator voltage of the grid is proposed. Following standard convention, all electrical (two–dimensional vector) signals are partitioned into their so–called  $d$  and  $q$  components. This yields the electrical equations

$$L_s \frac{di_{sd}}{dt} + L_{sr} \frac{di_{rd}}{dt} = -R_s i_{sd} + \omega_s L_s i_{sq} + \omega_s L_{sr} i_{rq} + v_{sd} \quad (6)$$

$$L_s \frac{di_{sq}}{dt} + L_{sr} \frac{di_{rq}}{dt} = -\omega_s L_s i_{sd} - R_s i_{sq} - \omega_s L_{sr} i_{rd} + v_{sq} \quad (7)$$

$$L_{sr} \frac{di_{sd}}{dt} + L_r \frac{di_{rd}}{dt} = (\omega_s - \omega) L_{sr} i_{sq} - R_r i_{rd} + (\omega_s - \omega) L_{sr} i_{rq} + v_{rd} \quad (8)$$

$$L_{sr} \frac{di_{sq}}{dt} + L_r \frac{di_{rq}}{dt} = -(\omega_s - \omega) L_{sr} i_{sd} - (\omega_s - \omega) L_{sr} i_{rd} - R_r i_{rq} + v_{rq} \quad (9)$$

where  $i_{sd}, i_{sq}, i_{rd}, i_{rq}$  are stator and rotor currents, respectively,  $v_{sd}, v_{sq}$  are the stator voltages,  $v_{rd}, v_{rq}$  are the rotor voltages (and play the role of the control inputs),  $\omega$  is the mechanical speed, and  $\omega_s$  is the stator frequency.  $R_s, R_r$  are the stator and rotor resistances,  $L_s, L_r$  and  $L_{sr}$  are the stator and rotor self–inductances and mutual inductance, with  $L_s L_r > L_{sr}^2$ .

The mechanical equation is given by

$$J\dot{\omega} = \tau_e - B_r \omega - \tau_L \quad (10)$$

where the electrical torque is

$$\tau_e = L_{sr}(i_{sq}i_{rd} - i_{sd}i_{rq}) \quad (11)$$

and  $J$  is the inertia,  $B_r$  is the friction coefficient, and  $\tau_L$  is an external constant torque.

The use of the stator-voltage oriented synchronous frame,  $v_{sd} = V_s$  and  $v_{sq} = 0$  (with  $V_s$  the amplitude of the three-phase stator voltage), allows us to express the stator active and reactive powers in terms of  $i_{sd}$  and  $i_{sq}$ , respectively, so that,

$$P_s = v_{sd}i_{sd} + v_{sq}i_{sq} \quad (12)$$

$$Q_s = v_{sq}i_{sd} - v_{sd}i_{sq} \quad (13)$$

simplify to

$$P_s = V_s i_{sd} \quad (14)$$

$$Q_s = -V_s i_{sq}. \quad (15)$$

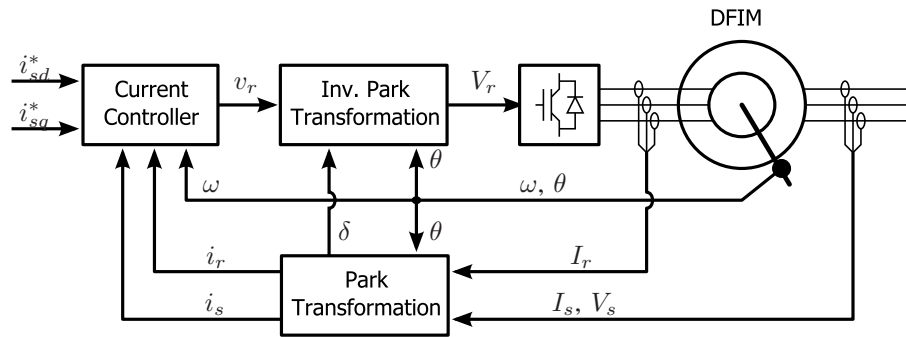


Fig. 2. Proposed control scheme for a DFIM.

In particular, assigning a desired value  $i_{sq}^*$  allows one to regulate the power factor of the stator side of the machine, while  $i_{sd}^*$  can be used to control the active power (delivered or consumed) by the DFIM. In a drive application,  $i_{sd}^*$  is fixed as a desired value to achieve the target torque in the presence of voltage constraints. This paper concentrates only on the problem of robust regulation of  $i_s$  to its desired value.

#### IV. FEEDBACK-LINEARIZING CURRENT CONTROLLER

The proposed control scheme is presented in Figure 2. It is composed of the current control block and the well-known Blondel-Park transformation to recover the dq-measurements of the currents and the stator voltages, and its inverse to generate the three-phase rotor voltages from the computed  $v_r$  values (in the dq-framework).

Thanks to the use of the stator voltage reference (already used in [12] or [1] among others) the proposed algorithm is simpler than the classic stator-flux oriented control [6], where the stator flux estimation (or reconstruction) is required for the reference frame orientation. Furthermore, the stator voltage oriented framework allows us to directly use the stator currents  $i_s$  to regulate the active and reactive stator power, see equations (14) and (15). This fact also simplifies the algorithm compared with the standard approach.

The control algorithm can be also used as the inner-current loop for drive applications. Fixing  $i_{sq}$  for the reactive power compensation, a suitable  $i_{sd}$  can be obtained from a mechanical outer-loop for the torque (using (11)), or speed regulation (from the mechanical dynamics (10)).

The transformation of the three phase (stator and rotor) currents to the synchronous-reference (aligned to the stator voltages) is achieved with the rotation matrix

$$e^{J_2\eta} = \begin{pmatrix} \cos(\eta) & -\sin(\eta) \\ \sin(\eta) & \cos(\eta) \end{pmatrix} \quad (16)$$

with  $\eta = \delta$  for the stator variables, where  $\delta$  is defined by the stator voltages and can be easily obtained via

$$\delta = \arctan\left(\frac{v_{s\beta}}{v_{s\alpha}}\right), \quad (17)$$

and  $\eta = \delta - \theta$  for the rotor ones, where  $\theta$  is the rotor position ( $\dot{\theta} = \omega$ ). Note that  $\dot{\delta} = \omega_s$ .

This part of the scheme is easier to implement than the stator-flux oriented control, which depends on the stator flux estimation.

### A. Feedback-linearizing current controller

The proposed controller consists of a feedback-linearization stage

$$v_{rd} = -(\omega_s - \omega)L_{sr}i_{sq} + R_r i_{rd} - (\omega_s - \omega)L_r i_{rq} + u_d \quad (18)$$

$$v_{rq} = (\omega_s - \omega)L_{sr}i_{sd} + (\omega_s - \omega)L_r i_{rd} + R_r i_{rq} + u_q \quad (19)$$

and a PI action

$$u_d = -k_P(i_{sq}^* - i_{sq}) - k_I \int (i_{sq}^* - i_{sq}) dt \quad (20)$$

$$u_q = k_P(i_{sd}^* - i_{sd}) + k_I \int (i_{sd}^* - i_{sd}) dt \quad (21)$$

with the scalar proportional and integral gains  $k_P$  and  $k_I$ , respectively.

*Remark 1:* The first three terms in (18) and (19) exactly cancel the first three terms in (8) and (9), respectively, feedback-linearizing the system and transforming the rotor equations to  $L_{sr} \frac{di_{sd}}{dt} + L_r \frac{di_{rd}}{dt} = u_d$  and  $L_{sr} \frac{di_{sq}}{dt} + L_r \frac{di_{rq}}{dt} = u_q$ .

*Remark 2:* In contrast to the standard practice, as mentioned in [1], the PI controller is defined relating the d-rotor voltage component with (minus) the error of the q-stator current (20), and the q-rotor voltage with (plus) the error of the d-stator current (21). This fact turns out to be critical for the stability analysis. As explained in [22], this structure was suggested by applying passivity-based nonlinear control techniques.

Substituting (18)-(19) in (8)-(9), a linear closed-loop system is obtained. Applying the Laplace transform, stability of the system is determined by a 6th order characteristic polynomial, which was analyzed in [16] but without reaching complete analytic conditions for stability. Interestingly, this sixth order characteristic polynomial with real coefficients can be reduced into a 3rd order polynomial with complex coefficients for which complete analysis is possible.

Defining  $\mathcal{I}_s(s) = I_{sd}(s) + jI_{sq}(s)$ ,  $\mathcal{I}_r(s) = I_{rd}(s) + jI_{rq}(s)$ ,  $\mathcal{V}_s(s) = V_{sd}(s) + jV_{sq}(s)$ ,  $\mathcal{V}_r(s) = V_{rd}(s) + jV_{rq}(s)$ , the closed loop system can be written as

$$\mathcal{A}(s) \begin{pmatrix} \mathcal{I}_s(s) \\ \mathcal{I}_r(s) \\ \mathcal{V}_r(s) \end{pmatrix} = \begin{pmatrix} \mathcal{V}_s(s) \\ 0 \\ j(k_P s + k_I)\mathcal{I}_s^*(s) \end{pmatrix} \quad (22)$$

where

$$\mathcal{A}(s) = \begin{pmatrix} L_s s + R_s + j\omega_s L_s & L_{sr} s + j\omega_s L_{sr} & 0 \\ L_{sr} s & L_r s & -1 \\ j(k_P s + k_I) & 0 & s \end{pmatrix}. \quad (23)$$

Notice that the polynomial  $\det \mathcal{A}(s)$  has 3 roots that are not required to be real or appear as complex pairs. The complex polynomial has the form

$$\det \mathcal{A}(s) = a_0 s^3 + (a_1 + j b_1) s^2 + (a_2 + j b_2) s + a_3 + j b_3 \quad (24)$$

where the parameter values are given in Appendix A.

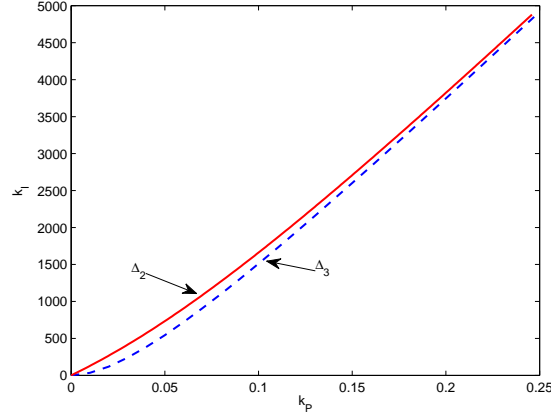


Fig. 3. Stability boundary for the proposed control law (18)-(19) as determined by  $\Delta_2$  and  $\Delta_3$ . The stable region is on the right side of the curve.

Now the stability of the closed loop system (6)-(9) with (18)-(19), can be analyzed with Lemma 1, where  $a_0 = \mu > 0$  ( $\mu = L_s L_r - L_{sr}^2 >$ , in all electrical machines) is fulfilled. Computing conditions (3)-(5) yields

$$\Delta_1 = L_r R_s \quad (25)$$

$$\Delta_2 = L_{sr} (k_P \omega_s L_r^2 R_s^2 + k_P k_I L_{sr} L_r R_s - 2k_I \omega_s \mu L_r R_s - k_I^2 \mu L_{sr}) \quad (26)$$

$$\Delta_3 = k_I \omega_s^3 L_{sr}^2 L_r R_s (k_P^2 L_{sr} L_r R_s - k_P k_I \mu L_{sr} - k_I \omega_s \mu^2). \quad (27)$$

The first condition is automatically fulfilled because  $L_r, R_s > 0$ . It can be shown (see Appendix B) that one must have  $k_I > 0$ , and the third condition is more restrictive than the second one. Consequently, the Hurwitz conditions reduce to  $\Delta_3 > 0$ . Notice that the stability condition does not depend on the mechanical speed. This stability condition has as asymptote the result presented in [16], which implies a generalization of the previous work. Figure 3 represents both conditions for the machine parameters used in Section VI.

*Proposition 1:* Consider the DFIM system (6)-(9) in closed-loop with the control law (18)-(19). If

$$0 < k_I < \frac{k_P^2 L_{sr} L_r R_s}{\mu (\mu \omega_s + k_P L_{sr})} \quad (28)$$

the closed-loop system is asymptotically stable.

*Proof:* See Appendix B. ■

Finally, it is worth mentioning that the PI gain selection can be done by analyzing (24) in order to place (some of) the poles at a desired location.

### B. Effect of unknown parameters

As seen from (18)-(19), the feedback linearization term requires the knowledge of  $R_r$ ,  $L_s$  and  $L_{sr}$ , which are in general uncertain and time-varying parameters. In particular, due to thermal effects, the value of  $R_r$  is highly varying. In order to evaluate the effect of a possibly incorrect estimation of  $R_r$ , let us assume that one uses in (18)-(19) an estimated value  $\hat{R}_r$ ,

which can differ from the actual value of the rotor resistance. Then, (23) slightly modifies to

$$\mathcal{A}_r(s) = \begin{pmatrix} L_s s + R_s + j\omega_s L_s & L_{sr} s + j\omega_s L_{sr} & 0 \\ L_{sr} s & L_r s + \tilde{R}_r & -1 \\ j(k_P s + k_I) & 0 & s \end{pmatrix}, \quad (29)$$

where  $\tilde{R}_r = R_r - \hat{R}_r$ .

Applying again Lemma 1 to the new matrix  $\mathcal{A}_r(s)$ , it is possible to obtain a set of conditions given by  $\Delta_1, \Delta_2, \Delta_3 > 0$ . The determinant of  $\mathcal{A}_r(s)$  still has the form of (24), with the same parameters of Appendix A except for the following three:

$$a_1 = L_r R_s + L_s \tilde{R}_r \quad (30)$$

$$a_2 = k_P \omega_s L_{sr} + R_s \tilde{R}_r \quad (31)$$

$$b_2 = -k_I L_{sr} + \omega_s L_s \tilde{R}_r \quad (32)$$

First, note that  $a_1 > 0$ , and consequently  $\Delta_1 > 0$ , if and only if  $\hat{R}_r < R_r + \frac{L_r}{L_s} R_s$ , which warns against an overestimation of  $R_r$ . Conditions  $\Delta_2 > 0$  and  $\Delta_3 > 0$  are quite more complicated,

$$\Delta_2 = c_1 k_I^2 + c_2 k_P k_I + c_3 k_I + c_4 k_P + c_5 \quad (33)$$

$$\Delta_3 = d_1 k_I^3 + d_2 k_P k_I^2 + d_3 k_I^2 + d_4 k_P^2 k_I + d_5 k_P k_I + d_6 k_I \quad (34)$$

where the parameters are detailed in Appendix C.

At this point, in order to simplify the stability conditions, it is possible to compute the positive slope asymptotes of (33) and (34), which turn out to be the same and given by

$$k_I = \frac{L_r R_s + L_s \tilde{R}_r}{\mu} k_P - \frac{\omega_s L_r R_s}{L_{sr}}. \quad (35)$$

Notice that for  $\tilde{R}_r = 0$ , this corresponds to the asymptote of (28), and the stability condition presented in [16] is recovered. Also, it is worth mentioning that negative values for  $\hat{R}_r$  will increase the slope of (35) which implies a larger stability region. However, this selection will affect the performance of the controller with a longer stabilization time.

Figure 4, shows a numerical example of the stability region for different values of  $\hat{R}_r$ . With the parameters of the machine described in Section VI, and considering a 10% error in the  $R_r$  estimation,  $\Delta_3 > 0$  is more restrictive than  $\Delta_2 > 0$ . In Figure 4, the  $\Delta_3 = 0$  for different errors in the rotor resistance estimation are shown.

This numerical example shows that a positive error, *i.e.*  $\tilde{R}_r > 0$ , in the estimation of  $\hat{R}_r$  is preferred. In other words, overestimating the rotor resistance implies decreasing the stability region and, as pointed out before, can even destabilize the system. Moreover, for small values of  $\tilde{R}_r$ , a small stable region appears for  $k_P < 0$ . This can be easily seen from the asymptote (35), where  $\tilde{R}_r < 0$  implies a lower slope. This fact suggests taking  $\hat{R}_r = 0$  to have a larger stability region, and also simplify

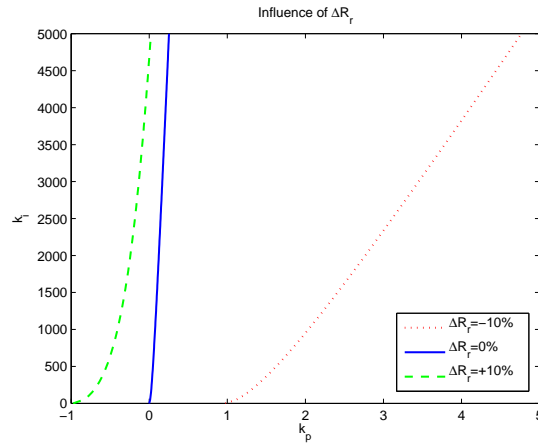


Fig. 4. Stability boundary for the proposed control law (18)-(19) with an uncertain value of  $R_r$ .

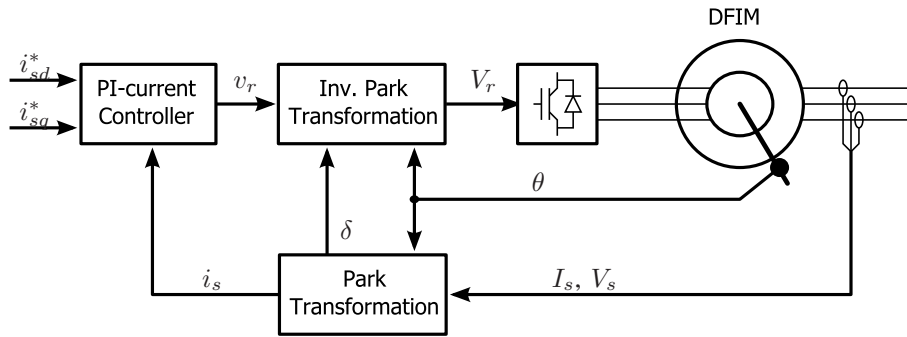


Fig. 5. Simplified control scheme for a DFIM.

the control law. Then, asymptote (35) yields,

$$k_I = \frac{L_r R_s + L_s R_r}{\mu} k_P - \frac{\omega_s L_r R_s}{L_{sr}}. \quad (36)$$

## V. PI STATOR CURRENT CONTROLLER

The control law introduced in the previous section guarantees stability for a large range of the PI parameter values. However, in order to implement the control algorithm, it is necessary to know some machine parameters and both the stator and the rotor currents. In this section, a simplification of the proposed controller (18)-(19) is analyzed, that only keeps the PI action, i.e.,

$$v_{rd} = -k_P(i_{sq}^* - i_{sq}) - k_I \int (i_{sq}^* - i_{sq}) dt \quad (37)$$

$$v_{rq} = k_P(i_{sd}^* - i_{sd}) + k_I \int (i_{sd}^* - i_{sd}) dt \quad (38)$$

For this scheme, shown in Figure 5, the rotor currents are not required, and only the stator currents need to be measured. Notice that, in a torque controller application (see (11)), the rotor currents could be required to set the  $i_d^*$  value in an outer control loop.

At this point, for the stability analysis, a constant mechanical speed is assumed. Using the same idea as before, the closed-loop

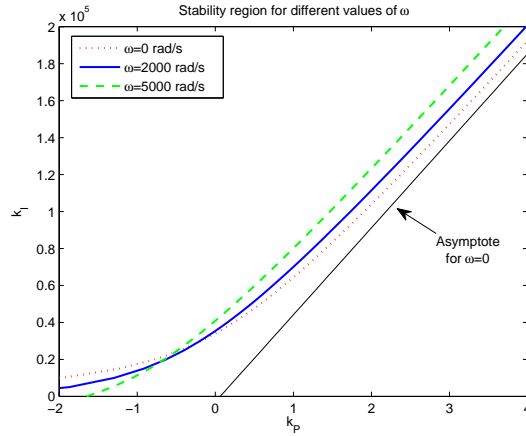


Fig. 6. Stability region for the proposed control law (37)-(38) for different values of  $\omega$ .

dynamics can be written as (22) with  $\mathcal{A}(s)$  becoming

$$\mathcal{A}_{PI}(s) = \begin{pmatrix} L_s s + R_s + j\omega_s L_s & L_{sr} s + j\omega_s L_{sr} & 0 \\ L_{sr} s + j(\omega_s - \omega)L_{sr} & L_r s + R_r + j(\omega_s - \omega)L_r & -1 \\ j(k_P s + k_I) & 0 & s \end{pmatrix}. \quad (39)$$

The polynomial  $\det \mathcal{A}_{PI}(s)$  still has 3 roots, and the Hurwitz test described in Lemma 1 can be used. The determinant of (39) has the same form as (24) with the coefficients given in Appendix D.

The stability of the closed loop system (6)-(9) with (37)-(38) can be analyzed by computing  $\Delta_1$ ,  $\Delta_2$ ,  $\Delta_3$ .  $\Delta_1 = a_1$  so that  $\Delta_1 > 0$ , while  $\Delta_2$  and  $\Delta_3$  are in the same form as (33) and (34), respectively, where the coefficients now take the values given in Appendix E.

To obtain an expression for the stability region becomes complicated. As a first result, conditions can be plotted for a numerical case. Using the machine parameters of Section VI, equations (33) and (34) are obtained for different values of the mechanical speed. Figure 6 shows the stability regions for the mechanical speed.

In order to bound the stability region, it is possible to find the asymptote of (33) and (34). Similarly to the case for an unknown rotor resistance presented in the previous section, the asymptotes for the  $\Delta_2 = 0$  and  $\Delta_3 = 0$  are equal and given by

$$k_I = \frac{L_r R_s + L_s R_r}{\mu} k_P + \frac{\omega L_s R_r - \omega_s (L_r R_s + L_s R_r)}{L_{sr}}. \quad (40)$$

Note that the slope of the stability boundary does not depend on the mechanical speed. As the worst case is when  $\omega = 0$ , the stability for the PI controller proposed can be ensured by setting

$$k_I < \frac{L_r R_s + L_s R_r}{\mu} k_P - \frac{\omega_s (L_r R_s + L_s R_r)}{L_{sr}}. \quad (41)$$

## VI. SIMULATIONS

The proposed controller was tested in numerical experiments using Matlab. In order to obtain an accurate simulation of the real plant, the model was built with the SimPowerSystems toolbox, and effects due to a digital implementation were considered.

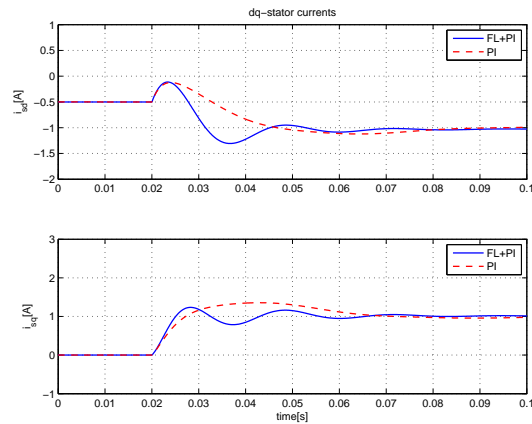


Fig. 7. Simulation results: stator currents under a change in the references, from  $i_s^* = [-3, 0]$ A to  $i_s^* = [-5, 1]$ A.

The DFIM parameters are the same than ones used in Section VII. The DFIM is connected to a 380V and 50Hz power grid that using a power preserving transformation and the stator-voltage oriented frame, this corresponds to a constant stator voltage vector  $v_s = [380, 0]$ V and  $\omega_s = 100\pi\text{rad s}^{-1}$ .

A first simulation consists in a comparison between the two presented control schemes. For this test, the dq-model (6)-(9) is in a closed loop with the control schemes (18)-(19) and (37)-(38). The knowledge of all the parameters is assumed for the feedback linearizing control scheme and the control gains of the PI action are fixed at  $k_P = 5$ ,  $k_I = 50$  in both cases. The mechanical speed is set to  $\omega = 325\text{rad s}^{-1}$  and the initial conditions are  $i_s(0) = [-0.5, 0]$ A. First, the reference is changed from the initial value to  $i_s^* = [-1, 1]$ A at  $t = 0.02\text{s}$ . As shown in Figure 7, both algorithms perform in a similar way. This result suggests the use of the direct PI controller because it is easily implementable; rotor currents are not needed, and the knowledge of the machine parameters is not required. However, the stability of the control law (37)-(38) is based on the assumption of constant mechanical speed. In the simulation depicted in Figure 8, the current references are  $i_s^* = [-3, 0]$ A and the mechanical speed is modified as follows: a step from  $300\text{rad s}^{-1}$  to  $295\text{rad s}^{-1}$  at  $t = 0.1\text{s}$ , and then a ramp with  $50\text{rad s}^{-2}$  and  $-50\text{rad s}^{-2}$  slope, from  $t = 0.3\text{s}$  to  $t = 0.5\text{s}$ , and  $t = 0.5\text{s}$  to  $t = 0.7\text{s}$ , respectively. When a sudden change of the velocity occurs, both d and q stator currents reach the desired values after a short time. Also, note that during the acceleration of the mechanical speed (from  $t = 0.3\text{s}$  to  $t = 0.7\text{s}$ ), the d-stator current tracks the reference value, but the q-stator current has some steady-state error.

The second test compares the proposed method (the so-called direct PI controller) with an existing PQ control which also uses the stator voltage oriented frame and splits the problem in two loops: a first rotor current loop, and an outer power control loop, see details in [13], pp. 2-18 to 2-22. At this point, two main differences arises with respect to the proposed controller (37)-(38): the stability of the PQ method is based on the assumption of a fast inner loop with respect the power control loop, and the use of current sensors for the rotor side is required. Figure 9, compares the behavior of the stator currents using the proposed algorithm versus the PQ control approach in [13], where the control gains were set to  $k_{Pp} = 1$ ,  $k_{Ip} = 150$  (for the PQ controller) and  $k_{Pc} = 10$ ,  $k_{Ic} = 1$  (for the rotor current controller). Notice that performance is similar although the proposed control law is easier to implement and less complex.

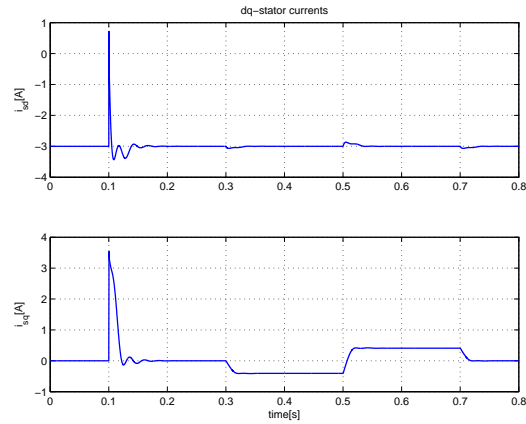


Fig. 8. Simulation results: stator currents under a change of the mechanical speed, from  $300\text{rads}^{-1}$  to  $295\text{rads}^{-1}$  at  $t = 0.1\text{s}$ , and acceleration of  $50\text{rads}^{-2}$  and  $-50\text{rads}^{-2}$ , from  $t = 0.3\text{s}$  to  $t = 0.5\text{s}$ , and  $t = 0.5\text{s}$  to  $t = 0.7\text{s}$ , respectively.

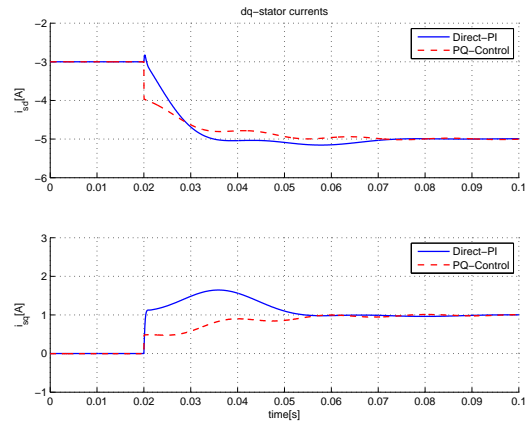


Fig. 9. Simulation results: comparison of the direct PI-controller algorithm with the stator voltage PQ control.

The third set of simulations test the so-called direct PI controller. In this case, the model is implemented using the SimPowerSystems toolbox of Matlab, which contains a library with realistic implementations of some elements such as sources, electrical machines and measurement elements. For this simulation, the Blondel-Park transformations had to be coded, as well as the obtained control action,  $v_r$ , that is converted to the three-phase voltage,  $V_r$ , to be applied to the rotor side of the DFIM. Also, the effects of a real implementation are included, *i.e.* sampling, quantification and saturation. The sampling frequency is set at 10kHz, all the variables are quantified as in a 16bit processor, and the rotor voltages which are saturated at  $\pm 120\text{V}$ , are delayed with one sampling time period. The control parameters and the mechanical speed are  $k_P = 1$ ,  $k_I = 150$  and  $\omega = 325\text{rads}^{-1}$ . The desired dq-stator currents are shown in Figure 10, where several scenarios are considered changing the stator current references,  $i_{sd}$  and  $i_{sq}$  (also simultaneously, at  $t = 1.5\text{s}$ ). Note that the reference change at  $t = 3.5\text{s}$  implies a switch of the power flow direction (from generating to absorbing).

Stator currents are depicted in Figures 11 and 12. The evolution of the measured three-phase stator currents are displayed in Figure 11. Figure 12 shows how the obtained dq-stator currents stabilize at the desired values under several reference changes. It is worth mentioning that the controller is able to operate for both signs of the  $i_{sd}$  current, showing that this algorithm can

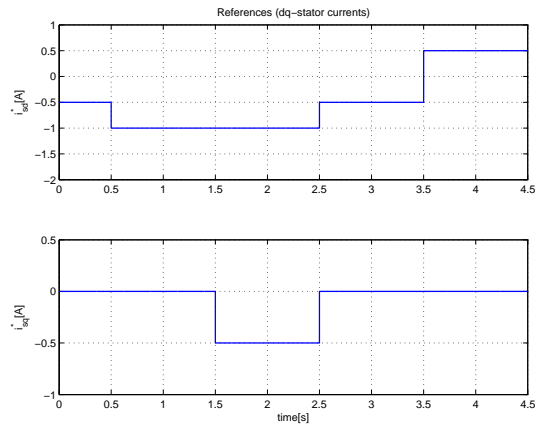


Fig. 10. Simulation results: dq-stator current references.

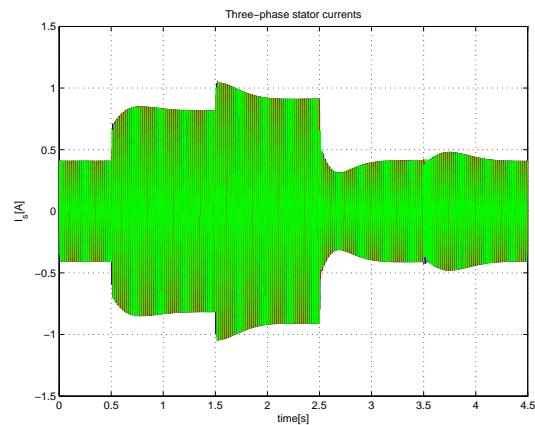


Fig. 11. Simulation results: three-phase stator currents.

be used for both generation of either electrical power or mechanical power (as in driving applications).

Figure 13 contains a detailed zoom for each reference change for the a-phase stator voltage and current in steady state. One can see how the phase changes depending on the value of the q-stator current component. The first step at  $t = 0.5$  s only modifies the current amplitude and the phase remains in opposite phase (power is flowing out of the DFIM, that is, the DFIM is in generation mode). The second change, at  $t = 1.5$  s, implies that some reactive power appears. The third reference change ( $t = 2.5$  s) returns to zero reactive power and reduces the active power delivered. Finally, the fourth change ( $t = 3.5$  s) affects only the direction of the power flow, with zero reactive power (voltage and current are in phase, or in opposite phase), and the current amplitude is kept. Overall, active power and reactive power can be regulated independently.

In order to evaluate the overall performance, the rotor voltages and currents are shown in Figures 14 and 15. The dq-rotor voltages allows to verify that the control signals provided by the algorithm are suitable for a final implementation. The behavior of the rotor currents shows that the other internal variables also stabilize in steady state.

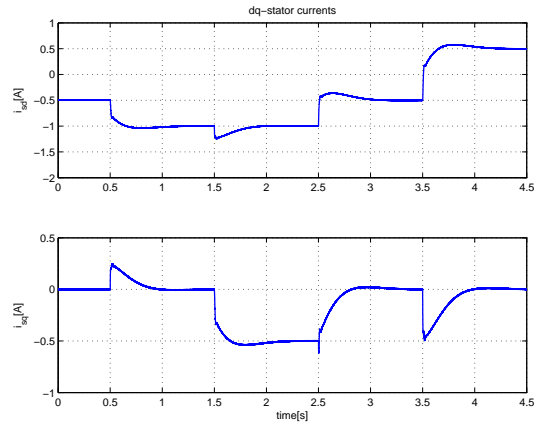


Fig. 12. Simulation results: dq-stator currents.

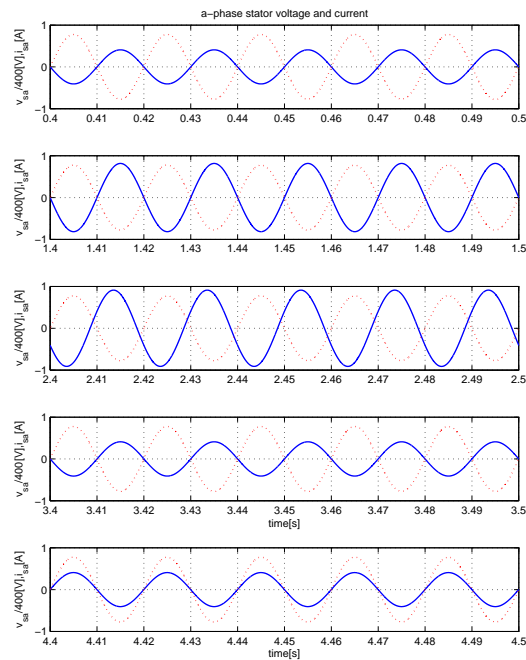


Fig. 13. Simulation results: detail of the a-phase stator voltage and current in steady state .

## VII. EXPERIMENTAL RESULTS

The proposed controller has been tested in a real plant. The DFIM is a 1.1kVA, 2 poles three-phase machine (DeLorenzo DL 1022K), with the following parameters:  $R_s = 4.92\Omega$ ,  $R_r = 4.42\Omega$ ,  $L_s = 725\text{mH}$ ,  $L_r = 715\text{mH}$  and  $L_m = 710\text{mH}$ . The DFIM is dragged by a 3kW DC motor with the 4Q2 commercial speed controller from Control Techniques Drives Ltd., used to provide a constant speed (at 2950rpm).

The control algorithm is programmed into a Texas Instruments floating point 150Mhz Digital Signal Processor (DSP TMS 320F28335). The DSP has 16 ADC channels with 12-bit resolution, with a maximum conversion speed of 12.5 MSPS, 6 PWM and 6 HRPWM outputs and 88 GPIO pins which can be used for communication purposes.

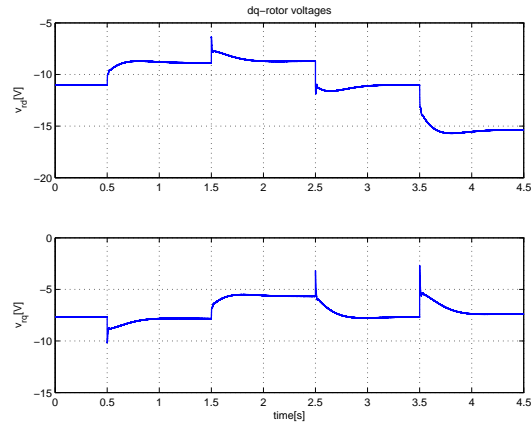


Fig. 14. Simulation results: dq-rotor voltages.

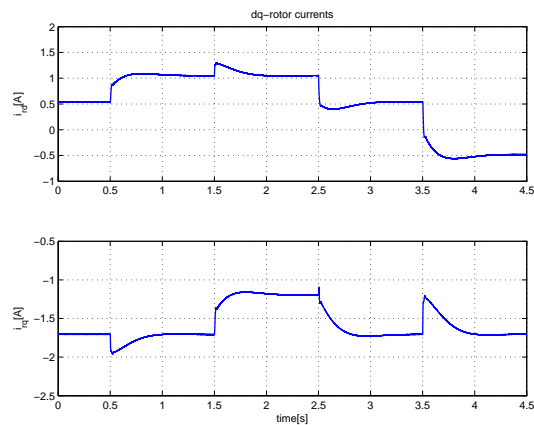


Fig. 15. Simulation results: dq-rotor currents.

Assuming a balanced grid, by using two voltage differential sensors and two hall effect currents sensors, the three phase stator voltages and currents are measured. Position is measured as well in order to compute the dq transformation. These measures are acquired by the DSP which is programmed from a personal computer. Real Time Workshop C code generation from Matlab/Simulink is used to implement dq- transformation and the control algorithm. The sample time is fixed to  $10^{-4}$ s, which corresponds to 10kHz as a maximum frequency.

First test corresponds to a change on the d-stator current component (related to the active power). The DFIM starts with references at  $i_s^* = [0.5, 0]$ A and are changed to  $i_{sd}^* = 0.5$ A. Figure 16 shows the stator voltage and current for the a-phase. Note that as the reactive power in the stator side is zero ( $i_{sq} = 0$ ), the stator voltage and current are in phase. Figure 17 shows the transient of the dq-stator currents and its references. Small oscillations of the transformed dq-currents corresponds to the effect of unbalanced phases of the actual machine. As in the simulation tests, the controller is able to control the active power by means of the d-stator current component. However, the transients of the stator currents is worst than the ones obtained in the simulations due to the interaction between the control required to keep the mechanical speed of the DC machine and the tested control algorithm. The steady state at  $i_{sq}^*$  is depicted in Figure 18 and shows that the a-phase stator current is zero.

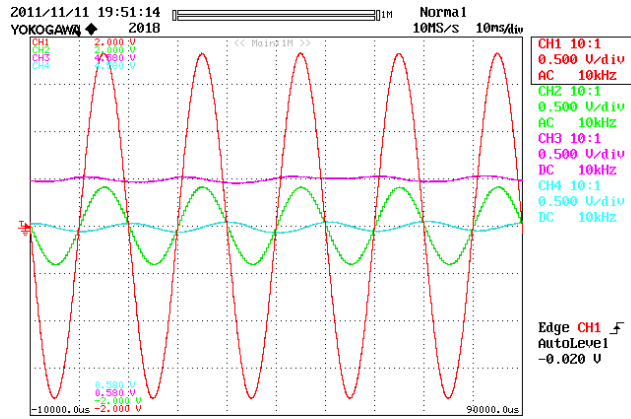


Fig. 16. Experimental results: a-phase stator voltage (CH1), a-phase stator current (CH2), d-stator current (CH3) and q-stator current (CH4), for  $i_s^* = [0.5, 0]A$ .

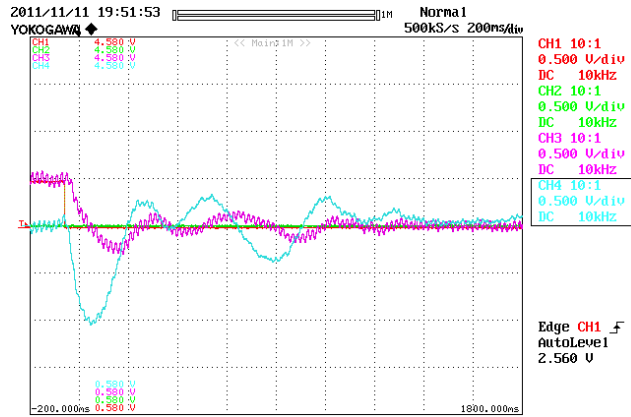


Fig. 17. Experimental results: dq-stator currents for a change reference from  $i_s^* = [0.5, 0]A$  to  $i_s^* = [0, 0]A$ . (CH1): d-stator current reference. (CH2): q-stator current reference. (CH3): d-stator current. (CH4): q-stator current.

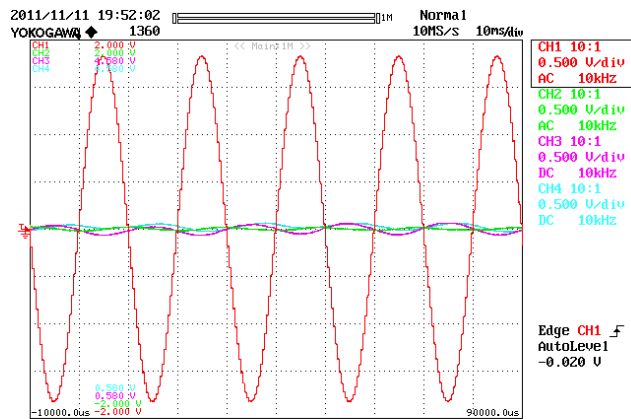


Fig. 18. Experimental results: a-phase stator voltage (CH1), a-phase stator current (CH2), d-stator current (CH3) and q-stator current (CH4), for  $i_s^* = [0, 0]A$ .

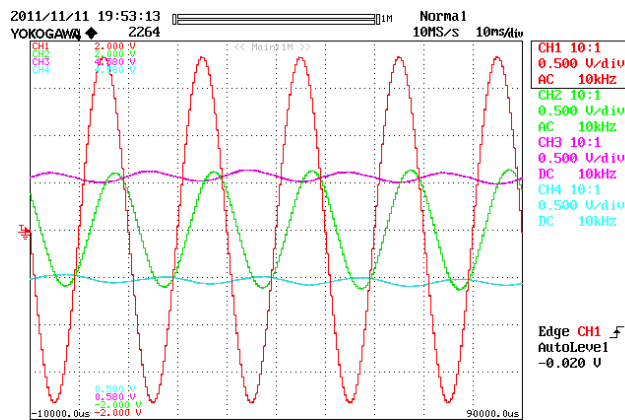


Fig. 19. Experimental results: a-phase stator voltage (CH1), a-phase stator current (CH2), d-stator current (CH3) and q-stator current (CH4), for  $i_s^* = [0.5, -0.5]$ A.

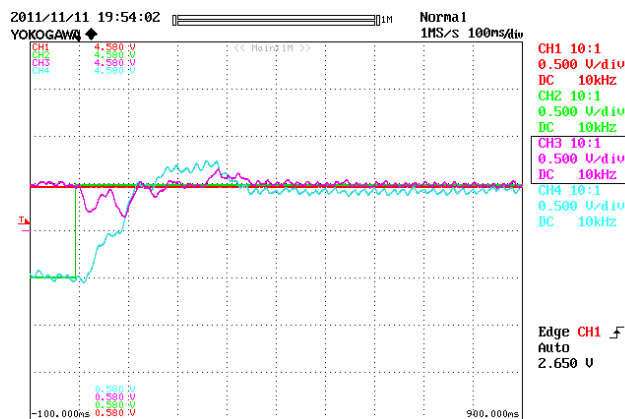


Fig. 20. Experimental results: dq-stator currents for a change reference from  $i_s^* = [0.5, 0.5]$ A to  $i_s^* = [0.5, -0.5]$ A. (CH1): d-stator current reference. (CH2): q-stator current reference. (CH3): d-stator current. (CH4): q-stator current.

The second test consists in to modify the reactive power of the DFIM. In this case the q-stator current component changes from  $i_s^* = [0.5, -0.5]$ A to  $i_s^* = [0.5, 0.5]$ A. Figure 19 shows the a-phase stator voltage and current at the beginning of the test where the phase of the current lags that of the voltage. The dq-stator currents behavior is shown in Figure 20. This test shows that the reactive power can be modified using the q-stator current component. Finally, the a-phase stator voltage and current in steady state are in Figure 21. In this case, the voltage lags the current.

## VIII. CONCLUSIONS

In this paper, a particularly simple controller for the DFIM was presented. It consists of a PI regulator for the stator currents and (possibly) a feedback linearizing term. As the proposed scheme is defined in the stator voltage reference frame, the active and reactive powers are directly related to the d and q stator currents, respectively, and the power regulation does not require extra loops or computations. Moreover, no stator flux estimation is required. Consequently, the algorithm is simpler than classical vector control.

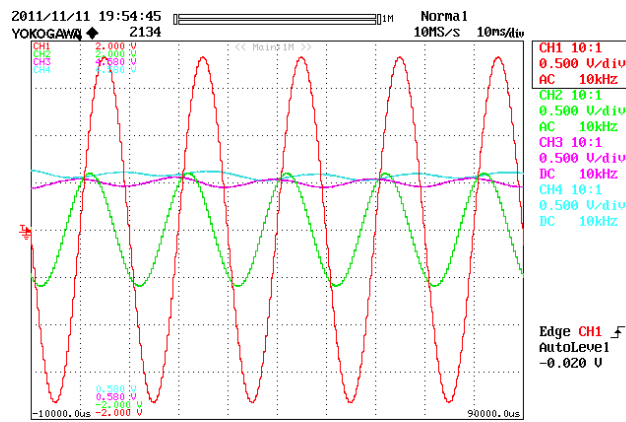


Fig. 21. Experimental results: a-phase stator voltage (CH1), a-phase stator current (CH2), d-stator current (CH3) and q-stator current (CH4), for  $i_s^* = [0.5, 0.5]A$ .

In contrast with the standard decoupling controllers, the PI action is defined with a particular structure (relating the d-rotor voltage component with (minus) the error of the q-stator current, and the q-rotor voltage with (plus) the error of the d-stator current). Stability is analyzed with a Routh-Hurwitz test for polynomials with complex coefficients. This method provides a simple analysis tool to determine the stability regions of the control gains.

The paper presents two approaches. The first algorithm consists of a feedback linearization stage plus a PI action. This scheme is particularly attractive because the resulting system is linear and independent of the mechanical speed. The influence of an incorrect estimation of the rotor resistance is also studied. The second algorithm only uses the PI term, so that it is extremely easy to implement. This current loop does not require either the knowledge of the machine parameters or measurements of the rotor currents. As opposed to the previous algorithm, the stability of the second approach is based on the assumption of constant mechanical speed. However, this restriction is widely assumed and can be accepted when the time constant of the mechanical dynamics is much higher than the electrical one.

The proposed controllers are verified in simulations. First, a dq-model of the DFIM is used to compare both controllers, resulting in a similar behavior. Secondly, a comparison is done with respect to the common PQ control and results that the presented algorithm is easy to tune and cheaper to implement because it does not require sensors for the rotor currents. And third, the direct PI algorithm is tested in a more accurate scenario. The model used in the simulation contains some parasitic elements and non-ideal effects such as sampling, quantification and some delay, in order to emulate a real experiment. The result, demonstrate good performance and validate the proposed control scheme.

Finally, some experimental results using the direct PI algorithm for a real setup are provided. These experimental tests confirm the advantages expected during the simulation stage.

Future research will include the problem of tracking currents, specially in applications with a non-constant profile references.

#### ACKNOWLEDGEMENTS

The authors would like to express their gratitude to R. Cardoner, E. Miró and V. Repecho for its help during the experimental implementation of the controller.

## REFERENCES

- [1] H. Akagi and H. Sato. Control and performance of a doubly-fed induction machine intended for a flywheel energy storage system. *IEEE Trans. on Power Electronics*, 17(1):109–116, 2002.
- [2] C. Batlle, A. Dòria-Cerezo, and R. Ortega. Power Flow Control of a Doubly-Fed Induction Machine Coupled to a Flywheel. *European Journal of Control*, 11(3):209–221, 2005.
- [3] L.L. Lai and T.F. Chan. *Distributed generation: Induction and permanent magnet generators*. Wiley & Sons, 2007.
- [4] M.G. Simoes and F.A. Farret. *Renewable energy systems: design and analysis with induction generators*. CRC Press, Boca Raton, 2004.
- [5] S. Müller, M. Deicke, and R.W. De Doncker. Doubly fed induction generator systems for wind turbines. *IEEE Industry Applications Magazine*, 8(3):26–33, 2002.
- [6] R. Peña, J.C. Clare, and G.M. Asher. Doubly fed induction generator using back-to-back pwm converters and its application to variable speed wind-energy generation. In *IEEE Proc. Electric Power Applications*, volume 143-5, pages 231–241, 1996.
- [7] A. Petersson, L. Harnfors, and T. Thiringer. Evaluation of current control methods for wind turbines using doubly-fed induction machines. *IEEE Trans. on Power Electronics*, 20(1):227–235, 2005.
- [8] C. Batlle, A. Dòria-Cerezo, G. Espinosa-Pérez, and R. Ortega. Simultaneous interconnection and damping assignment passivity-based control: the induction machine case study. *International Journal of Control*, 82(2):241–255, 2009.
- [9] W. Leonhard. *Control of electric drives*. Springer, 1995.
- [10] A. Tapia, G. Tapia, J. X. Ostolaza, and J. R. Sáenz. Modeling and control of a wind turbine driven doubly fed induction generator. *IEEE Trans. on Energy Conversion*, 18:194–204, 2003.
- [11] J. Hu, H. Nian, B. Hu, and Z.Q. Zhu Y. He. Direct active and reactive power regulation of DFIG using sliding-mode control approach. *IEEE Trans. on Energy Conversion*, 25(4):1028–1039, 2010.
- [12] M. Yamamoto and O. Motoyoshi. Active and reactive power control for doubly-fed wound rotor induction generator. *IEEE Trans. on Power Electronics*, 24(3):758–765, 1991.
- [13] I. Boldea. *Variable speed generators*. CRC Press, 2006.
- [14] B. Mwinyiwiwa, Y. Zhang, B. Shen, and B.T. Ooi. Rotor position phase-locked loop for decoupled P-Q control of DFIG for wind power generation. *IEEE Trans. on Energy Conversion*, 24(3):758–765, 2009.
- [15] E. Frank. On the zeros polynomials with complex coefficients. *Bulletin of the American Mathematical Society*, 5(2):144–157, 1946.
- [16] C. Batlle, A. Dòria-Cerezo, and R. Ortega. A Robustly Stable PI Controller for the Doubly-fed Induction Machine. In *Proc. 32nd Annual Conference of the IEEE Industrial Electronics Society (IECON)*, pages 5113–5118, 2006.
- [17] M. Bodson and O. Kiselychuk. Analytic conditions for spontaneous self-excitation in induction generators. In *Proc. of the American Control Conference*, 2010.
- [18] S. Peresada, A. Tilli, and A. Tonelli. Power control of a doubly fed induction machine via output feedback. *Control Engineering Practice*, 12:41–57, 2004.
- [19] M. Bodson. The complex hurwitz test for the stability analysis of induction generators. In *Proc. of the American Control Conference*, 2010.
- [20] J. Chiasson. *Modeling and High Performance Control of Electric Machines*. John Wiley & Sons Inc., 2005.
- [21] P.C. Krause. *Analysis of electric machinery*. McGraw-Hill, 1986.
- [22] A. Dòria-Cerezo. *Modeling, simulation and control of a doubly-fed induction machine controlled by a back-to-back converter*. PhD thesis, Universitat Politècnica de Catalunya, 2006. Available on-line: <http://www.tdx.cat/handle/10803/5945>.

## APPENDIX

**Appendix A: Parameters of the complex polynomial  $\det \mathcal{A}(s)$  in Subsection IV-A.** Parameters of (24) in Subsection IV-A are

$$a_0 = \mu \quad (42)$$

$$a_1 = L_r R_s \quad (43)$$

$$b_1 = \omega_s \mu - k_P L_{sr} \quad (44)$$

$$a_2 = k_P \omega_s L_{sr} \quad (45)$$

$$b_2 = -k_I L_{sr} \quad (46)$$

$$a_3 = k_I \omega_s L_{sr} \quad (47)$$

$$b_3 = 0 \quad (48)$$

where  $\mu = L_s L_r - L_{sr}^2$ .

**Appendix B: Proof of Proposition 1.** From Lemma 1, the stability conditions are  $\Delta_1 > 0$  (automatically fulfilled due to  $L_r, R_s > 0$ ),  $\Delta_2 > 0$  and  $\Delta_3 > 0$ . The proof contains two parts. First, it is shown that, for  $k_I > 0$ , conditions (28) and  $k_P > 0$  are derived. Secondly, it is proved that there is no stability for negative values of  $k_I$ .

Let us start with the case  $k_I > 0$ . Since (28) comes from  $\Delta_3 > 0$ , the proof only requires to show that  $\Delta_2 > 0$  is satisfied whenever  $\Delta_3 > 0$  holds, and that  $k_P$  should be positive.

Note that  $\Delta_2 > 0$  if and only if

$$k_P > \frac{k_I \mu (2\omega_s L_r R_s + k_I L_{sr})}{L_r R_s (\omega_s L_r R_s + k_I L_{sr})}. \quad (49)$$

Furthermore, consider the function  $f(k_P)$  defined by

$$f(k_P) = k_P^2 L_{sr} L_r R_s - k_P k_I \mu L_{sr} - k_I \omega_s \mu^2 \quad (50)$$

and note that, with  $k_I > 0$ ,  $\Delta_3 > 0$  holds true if and only if  $f(k_P) > 0$ .  $f(k_P)$  is a quadratic function such that  $f(k_P) = 0$  for

$$k_P = \frac{k_I \mu L_{sr} \pm \sqrt{(k_I \mu L_{sr})^2 + 4k_I \omega_s \mu^2 L_{sr} L_r R_s}}{2L_{sr} L_r R_s}. \quad (51)$$

Given that there are two real roots, one positive and the other negative, and the later is inconsistent with (49), it follows that  $f(k_P) > 0$  if and only if

$$k_P > \frac{k_I \mu L_{sr} + \sqrt{(k_I \mu L_{sr})^2 + 4k_I \omega_s \mu^2 L_{sr} L_r R_s}}{2L_{sr} L_r R_s}, \quad (52)$$

which also implies  $k_P > 0$ .

The desired result is proved if it can be shown that (52) implies (49), *i.e.*

$$\frac{k_I \mu L_{sr} + \sqrt{(k_I \mu L_{sr})^2 + 4k_I \omega_s \mu^2 L_{sr} L_r R_s}}{2L_{sr} L_r R_s} > \frac{k_I \mu (2\omega_s L_r R_s + k_I L_{sr})}{L_r R_s (\omega_s L_r R_s + k_I L_{sr})}, \quad (53)$$

or, equivalently,

$$(\omega_s L_r R_s + k_I L_{sr})(k_I \mu L_{sr} + \sqrt{(k_I \mu L_{sr})^2 + 4k_I \omega_s \mu^2 L_{sr} L_r R_s}) > 2k_I \mu L_{sr}(2\omega_s L_r R_s + k_I L_{sr}). \quad (54)$$

this inequality is satisfied if

$$(\omega_s L_r R_s + k_I L_{sr})\sqrt{(k_I \mu L_{sr})^2 + 4k_I \omega_s \mu^2 L_{sr} L_r R_s} > 2k_I \mu L_{sr}(2\omega_s L_r R_s + k_I L_{sr}) - (\omega_s L_r R_s + k_I L_{sr})k_I \mu L_{sr} \quad (55)$$

or

$$\begin{aligned} & (\omega_s L_r R_s + k_I L_{sr})^2((k_I \mu L_{sr})^2 + 4k_I \omega_s \mu^2 L_{sr} L_r R_s) + 4(k_I \mu L_{sr})^2(2\omega_s L_r R_s + k_I L_{sr})(\omega_s L_r R_s + k_I L_{sr}) \\ & > 4(k_I \mu L_{sr})^2(2\omega_s L_r R_s + k_I L_{sr})^2 + (\omega_s L_r R_s + k_I L_{sr})^2(k_I \mu L_{sr})^2 \end{aligned} \quad (56)$$

or

$$4k_I \omega_s \mu^2 L_{sr} L_r R_s (\omega_s L_r R_s + k_I L_{sr})^2 > 4(k_I \mu L_{sr})^2(2\omega_s L_r R_s + k_I L_{sr})\omega_s L_r R_s \quad (57)$$

or

$$(\omega_s L_r R_s + k_I L_{sr})^2 > (k_I L_{sr})^2 + 2k_I \omega_s L_{sr} L_r R_s. \quad (58)$$

Since the last inequality is indeed always valid, we may conclude that, for  $k_I > 0$ ,  $\Delta_2 > 0$  implies that  $k_P > 0$ , and  $k_P > 0$  together with  $\Delta_3 > 0$  implies  $\Delta_2 > 0$ . Therefore  $\Delta_2 > 0, \Delta_3 > 0$  hold if, and only if,  $k_P > 0, \Delta_3 > 0$ , and the stability is determined by (28) and  $k_P > 0$ .

It is possible to show that for  $k_I < 0$  there does not exist a set of  $k_P$  values which satisfies simultaneously  $\Delta_2 > 0$  and  $\Delta_3 > 0$ . Solutions of  $\Delta_3 > 0$  with  $k_I < 0$  imply  $f(k_P) < 0$ . If

$$k_I < -\frac{4\omega_s L_r R_s}{L_{sr}}, \quad (59)$$

and equation (50) has two negative real solutions

$$k_{P1} = \frac{k_I \mu L_{sr} + \sqrt{(k_I \mu L_{sr})^2 + 4k_I \omega_s \mu^2 L_{sr} L_r R_s}}{2L_{sr} L_r R_s} \quad (60)$$

$$k_{P2} = \frac{k_I \mu L_{sr} - \sqrt{(k_I \mu L_{sr})^2 + 4k_I \omega_s \mu^2 L_{sr} L_r R_s}}{2L_{sr} L_r R_s}. \quad (61)$$

Solutions of  $f(k_P) < 0$  are bounded by  $k_{P2} < k_P < k_{P1}$ . On the other hand, from  $\Delta_2 > 0$ , inequality (59) implies

$$k_P < \frac{k_I \mu (2\omega_s L_r R_s + k_I L_{sr})}{L_r R_s (\omega_s L_r R_s + k_I L_{sr})}. \quad (62)$$

It can be shown that the constraint given by (62) does not contain the range  $k_{P2} < k_P < k_{P1}$ , i.e.

$$\frac{k_I \mu (2\omega_s L_r R_s + k_I L_{sr})}{L_r R_s (\omega_s L_r R_s + k_I L_{sr})} < \frac{k_I \mu L_{sr} - \sqrt{(k_I \mu L_{sr})^2 + 4k_I \omega_s \mu^2 L_{sr} L_r R_s}}{2L_{sr} L_r R_s}. \quad (63)$$

**Appendix C: Parameters of the  $\Delta_2$  and  $\Delta_3$  conditions in Subsection IV-B.** Parameters of (33) and (34) are

$$c_1 = -\mu L_{sr}^2 \quad (64)$$

$$c_2 = L_{sr}^2 (L_r R_s + L_s \tilde{R}_r) \quad (65)$$

$$c_3 = -2\omega_s \mu L_{sr} L_r R_s \quad (66)$$

$$c_4 = \omega_s L_{sr} L_r R_s (L_r R_s + L_s \tilde{R}_r) \quad (67)$$

$$c_5 = R_s \tilde{R}_r \left( (L_r R_s + L_s \tilde{R}_r)^2 + \omega_s^2 \mu L_s L_r \right) \quad (68)$$

and

$$d_1 = -\omega_s \mu L_{sr}^3 R_s \tilde{R}_r \quad (69)$$

$$d_2 = \omega_s L_{sr}^3 R_s \left( \tilde{R}_r (L_r R_s + L_s \tilde{R}_r) - \omega_s^2 \mu L_r \right) \quad (70)$$

$$d_3 = -\omega_s^2 \mu L_{sr}^2 R_s (L_s \tilde{R}_r^2 + \omega_s^2 \mu L_r + 3L_r R_s \tilde{R}_r) \quad (71)$$

$$d_4 = \omega_s^3 L_{sr}^3 L_r R_s (L_r R_s + L_s \tilde{R}_r) \quad (72)$$

$$d_5 = \omega_s^2 L_{sr}^2 R_s \tilde{R}_r \left( \omega_s^2 \mu L_s L_r + (L_r R_s + L_s \tilde{R}_r)^2 + L_r R_s (L_r R_s + L_s \tilde{R}_r) \right) \quad (73)$$

$$d_6 = \omega_s L_{sr} R_s^2 \tilde{R}_r^2 \left( \omega_s^2 \mu L_s L_r + (L_r R_s + L_s \tilde{R}_r)^2 \right) \quad (74)$$

**Appendix D: Parameters of the complex polynomial  $\det \mathcal{A}(s)$  in Section V.** Parameters of (24) in Section V are

$$a_0 = \mu \quad (75)$$

$$a_1 = L_r R_s + L_s R_r \quad (76)$$

$$b_1 = \mu(2\omega_s - \omega) - k_P L_{sr} \quad (77)$$

$$a_2 = R_s R_r - \omega_s(\omega_s - \omega)\mu + k_P \omega_s L_{sr} \quad (78)$$

$$b_2 = (\omega_s - \omega)L_r R_s + \omega_s L_s R_r - k_I L_{sr} \quad (79)$$

$$a_3 = k_I \omega_s L_{sr} \quad (80)$$

$$b_3 = 0. \quad (81)$$

**Appendix E: Parameters of the  $\Delta_2$  and  $\Delta_3$  conditions in Section V.** Parameters of (33) and (34) in Section V are

$$c_1 = -\mu L_{sr}^2 \quad (82)$$

$$c_2 = L_{sr}^2 (L_r R_s + L_s R_r) \quad (83)$$

$$c_3 = \mu L_{sr} (\omega (L_s R_r - L_r R_s) - \omega_s (L_r R_s + L_s R_r)) \quad (84)$$

$$c_4 = \omega L_{sr} L_r R_s (L_r R_s + L_s R_r) \quad (85)$$

$$c_5 = R_s R_r (L_r R_s + L_s R_r)^2 \quad (86)$$

and

$$d_1 = -\omega_s \mu L_{sr}^3 R_s R_r \quad (87)$$

$$d_2 = \omega_s L_{sr}^3 R_s (R_r (L_r R_s + L_s R_r) - \omega_s \omega \mu L_r) \quad (88)$$

$$d_3 = \omega_s \mu L_{sr}^2 R_s (-2\omega_s R_r (L_r R_s + L_s R_r) - \omega_s \omega^2 \mu L_r - \omega R_r (L_r R_s - L_s R_r)) \quad (89)$$

$$d_4 = \omega \omega_s^2 L_{sr}^3 L_r R_s (L_r R_s + L_s R_r) \quad (90)$$

$$d_5 = \omega \omega_s^2 \mu L_{sr}^2 L_r R_s (\omega L_s R_r - (\omega_s - \omega) (L_r R_s + L_s R_r)) \\ + \omega_s L_{sr}^2 R_s R_r (L_r R_s + L_s R_r) (\omega_s (L_r R_s + L_s R_r) + \omega L_r R_s) \quad (91)$$

$$d_6 = \omega_s L_{sr} R_s R_r (R_s R_r - (\omega_s - \omega) \omega_s \mu) ((L_r R_s + L_s R_r)^2 + \omega^2 \mu L_s L_r) \quad (92)$$